

Towards Micro-Plate Delivery using a re-sized Lab Automation Drone in High Throughput Systems

Dongbin Kim¹ and Paul Y. Oh²



Fig. 1. High Throughput Screening Laboratory(Tecan journal, 3-2007)

Abstract—In this paper, the author presents micro-plate grasping work using a re-sized lab automation drone in high throughput system. Here, a robotic arm is affixed to a rotorcraft. The arm's gripper allows the unmanned aerial vehicle to dexterously manipulate objects such as micro-arrays and test samples often used in high throughput systems (HTS). The result shows that drone could improve existing HTS operations. The 6 degree-of-freedom (DOF) arm and gripper design are deployed to pick and place microplae with different samples. Test-and-evaluation approach and results are also given.

I. INTRODUCTION

In lab automation, robots are broadly employed to accelerate sample handling (Fig. 1), such as in high throughput screening (HTS), in which manipulators and transfer lines quickly deliver micro-plates amongst numerous test stations. The net result is that a typical HTS system can handle over 500,000 samples a week. In the age of big data, higher throughput screening is significant for faster pharmaceutical development and hence quicker patent registrations and earlier market dive-in [1] [2].

However, once configured, they are not easily changed because it is usually custom-tailored to maximize throughput. This is important because as new tests emerge, older HTS systems cannot easily perform them. The National Institutes of Health (NIH) in the United States are looking at the potential of lab automation drones to add flexibility to existing HTS systems. Problems such as ground effect, limited battery life, and obstacle avoidance are indeed relevant to lab automation but also remain open research topics. The important

¹Dongbin Kim is with Drones and Autonomous Systems Laboratory (DASL), University of Nevada Las Vegas, NV 89119, USA dongbin.kim@unlv.edu

²Paul Y. Oh is with Drones and Autonomous Systems Laboratory (DASL), University of Nevada, Las Vegas, NV 89119, USA paul.oh@unlv.edu



Fig. 2. Re-sized Lab automation drone design

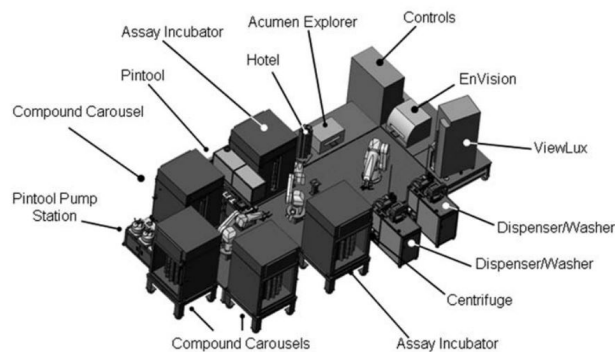


Fig. 3. NCGC robotic screening system

problem appears to be the lack of aerial manipulation arms and grippers for a lab automation drone. So, the author's previous work focused on 6-DoF parallel manipulator and sensorized parallel jaw gripper for a lab automation drone notional concept [3]. It results in about 95 percents precision at prototype pick-and-place. However, there is no actual micro-plate sample handling and the presented design is similar to or bigger than robotic arms in HTS. This paper thus presents micro-plate delivery using a smaller-sized mobile manipulating lab automation drone concept (see Fig. 2).

Section II describes related work; Section III details hardware and software components; Section IV showcases testing-and-evaluation results; and Section V presents conclusion and discusses future work.

II. RELATED WORK

Micro-plate delivery is important for HTS in big data era. There must be no fail. Therefore, today's state-of-the-art HTS employs many high-precision 6-DOF robot manipulators. Fig. 3 shows NIH Chemical Genomics Center(NCGC) robotic screening system [4]. Three Staubli (Duncan SC) robotic arms are mounted to execute biochemical and cell-based screening protocols [5]. These robots employ parallel jaw grippers to gently and precisely position and orient micro-plates.

The ability for aerial vehicles to manipulate or carry objects that they encounter has greatly expanded the types of missions achievable by unmanned aerial systems, such as aerial grasping, disaster response, casualty extraction, and personal assistance. Several configurations systems have been explored to create manipulation systems [6]-[9]. In the previous work from [3], the author chose to address parallel-mechanism arm for a lab automation drone, also with sensorized gripper for precise prototype grasping.

In spite of its precise positioning ability, the previous concept has issues to solve. First, the presented design hasn't delivered actual micro-plates with samples. And second, the design is bigger or similar to HTS robotic arms. Table. I shows the dimensions. Robotic arms move on pre-determined path by conveyor belts or rails, but drone has to fly. This means the design loses its mobility in HTS. Therefore, smaller-sized mobile manipulator and gripper design will be needed.

TABLE I

THE PREVIOUS CONCEPT AND HTS ROBOTIC ARM DIMENSIONS

| Dimensions | The previous Concept | TECAN Freedom EVO |
|------------|----------------------|-------------------|
| Height | 0.41 m | 0.87 m |
| Width | 1.25 m | 1.075 - 1.450 m |
| Depth | 1.25 m | 0.78 m |

III. HARDWARE AND SOFTWARE DESIGN

A. Mobility

To emulate rotorcraft drone motions, the 4-DOF gantry in Fig. 4 was built following Systems Integrated Sensor Test Rig(SISTR) from [10]. The gantry's

$$1.2m \times 0.5m \times 0.5m$$

workspace has the footprint to emulate a small HTS or a larger section of HTS. The gantry runs Dynamixel motors to provide end-effector cartesianal (x,y,z) position and yaw ψ orientation. The concept lab automation drone is affixed to the gantry's end-effector.

B. Parallel-Mechanism Manipulator Re-size

Previous 6-DOF parallel-mechanism was re-sized to control micro-plate positioning and orientation. In Fig. 5, the manipulator was designed with 8 legs attaching the base b to a moving platform p . Each leg has one driven revolute joint

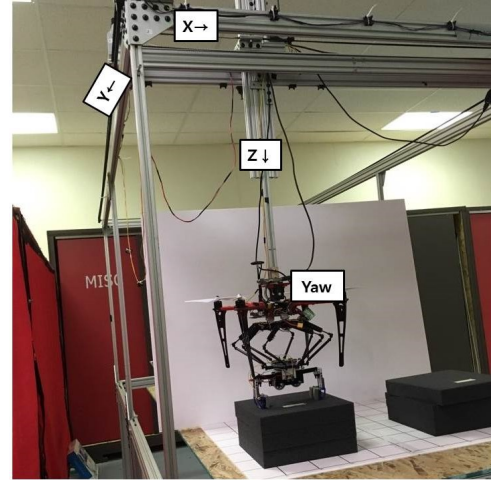


Fig. 4. The gantry crane system

TABLE II

PHYSICAL PROPERTIES OF THE MANIPULATOR CONCEPT DESIGN

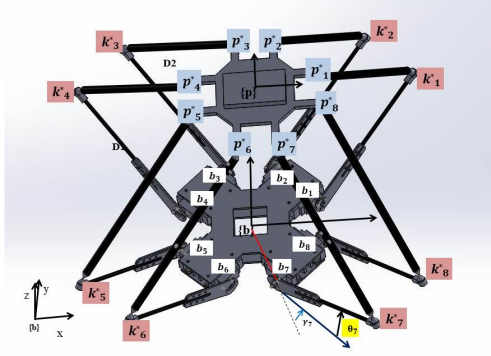
| Symbol | Value | Description |
|----------|----------|---|
| D_1 | 0.110 m | Fixed length link (base joint and knee) |
| D_2 | 0.135 m | Fixed length link (knee and top platform joint) |
| L | 0.773 m | Length (origin to the base attachment point) |
| M_{tm} | 0.471 kg | Total mass of manipulator concept design |
| M_{mm} | 0.093 kg | Total mass of moving components |

and two spherical joints (8-RSS). All 8 motors work together to drive the mass of the legs and the moving platform. Each leg, i , is attached to a servo on the base by a revolute joint. The servo drives a fixed length link, D_1 , to an angle θ_i from the plane of the base. The D_1 link is connected to a second fixed length link, D_2 , via a spherical "knee" joint, and the other end of the D_2 link attaches to the platform via a second spherical joint. The relative mounting positions of each leg is described in terms of angles ψ_{bi} and ψ_{pi} in the xy plane. γ_i is an angle between ψ_{bi} and the position of the link on the xy base plane, D_1 . Table III and IV shows the coordinates of each leg attachment point. All motors on the manipulator are controlled by the C++ open-source software, Pololu Mastro Servo Controller.

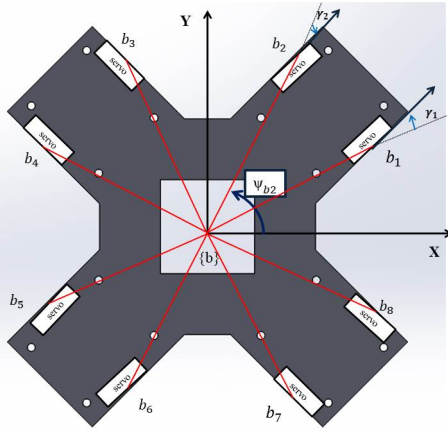
C. Parallel-Mechanism Manipulator Inverse Kinematics

The inverse kinematics for this parallel manipulator is calculated to identify goal angles for each of the 8 driven revolute joints around the base platform that will drive the top platform to a desired pose in the manipulator's base coordinates. The work in [3], [11], and [12] described RSS (Revolute-Spherical-Spherical).

The homogeneous transform bT_p is used to see each leg's attachment point to the top platform, p_i , to its goal pose p_i^*



(a) CAD Design of the manipulator



(b) Geometrical arrangement of leg attachment points



(c) Actual Design of the manipulator

Fig. 5. Re-sized parallel manipulator concept design (inverted for clarity)

in manipulator's base coordinates as shown in Eq. 1

$$p_i^* = p_i^b T_p \quad (1)$$

Next, the Euclidean distance L_i^* is calculated as the direct distance between b_i and p_i^* for each leg. L_i^* is a virtual leg, and it is the hypotenuse of the triangle formed by the points

TABLE III

ANGULAR COORDINATES OF LEG ATTACHMENT POINTS TO THE BASE AND MOVING PLATFORM

| Leg(i) | $\psi_{bi}(\text{radians})$ | $\gamma_i(\text{radians})$ | $\psi_{pi}(\text{radians})$ |
|------------|-----------------------------|----------------------------|-----------------------------|
| 1 | 0.3658 | 0.4196 | 0.2782 |
| 2 | 1.2050 | 0.4196 | 1.2926 |
| 3 | 1.9336 | 0.4196 | 1.8490 |
| 4 | 2.7758 | 0.4196 | 2.8634 |
| 5 | 3.5074 | 0.4196 | 3.4198 |
| 6 | 4.3466 | 0.4196 | 4.4342 |
| 7 | 5.0781 | 0.4196 | 4.9906 |
| 8 | 5.9194 | 0.4196 | 6.0050 |

TABLE IV

LEG ATTACHMENT POSITIONS TO THE TOP AND BASE IN MANIPULATOR BASE COORDINATES

| Leg(i) | Base Connections | | | Top Connections | | |
|------------|------------------|-------------|-------------|-----------------|-------------|-------------|
| | $b_{xi}(m)$ | $b_{yi}(m)$ | $b_{zi}(m)$ | $p_{xi}(m)$ | $p_{yi}(m)$ | $p_{zi}(m)$ |
| 1 | 0.0722 | 0.0277 | 0 | 0.0717 | 0.0205 | 0 |
| 2 | 0.0277 | 0.0722 | 0 | 0.0205 | 0.0717 | 0 |
| 3 | -0.0277 | 0.0722 | 0 | -0.0205 | 0.0717 | 0 |
| 4 | -0.0722 | 0.0277 | 0 | -0.0717 | 0.0205 | 0 |
| 5 | -0.0722 | -0.0277 | 0 | -0.0717 | -0.0205 | 0 |
| 6 | -0.0277 | -0.0722 | 0 | -0.0205 | -0.0717 | 0 |
| 7 | 0.0277 | -0.0722 | 0 | 0.0205 | -0.0717 | 0 |
| 8 | 0.0722 | -0.0277 | 0 | 0.0717 | -0.0205 | 0 |

b_i , p_i^* and the knee, m_i^* .

$$L_i^* = ||p_i^* - b_i|| \quad (2)$$

Finally, the desired angle of servo rotation, θ_i , is calculated by Eq. 3

$$\theta_i = \arcsin\left(\frac{c}{\sqrt{a^2 + b^2}}\right) - \arctan\left(\frac{b}{a}\right), \quad (3)$$

where:

$$\begin{aligned} a &= 2D_1(p_{zi}^* - b_{zi}) \\ b &= 2D_1[(p_{xi}^* - b_{xi}) \cos(\psi_{bi} \pm \gamma) + (p_{yi}^* - b_{yi}) \sin(\psi_{bi} \pm \gamma)] \\ c &= L_i^{*2} - D_2^2 + D_1^2. \end{aligned}$$

In b , the sum of the angles is used in the sinusoids for legs L_1, L_3, L_5 , and L_7 , while the difference of the angles is used for legs L_2, L_4, L_6 , and L_8 .

D. LEGO-Base Sensorized Parallel Jaw Gripper Re-size

TABLE V

PHYSICAL PROPERTIES OF THE GRIPPER CONCEPT DESIGN

| Symbol | Value | Description [m] |
|----------|--------------|--|
| W | 0.095-0.185m | Width between grip and non-grip |
| L | 0.11 m | Length of the gripper |
| M_{ig} | 0.234 kg | Total mass of the gripper concept design |

The sensorized parallel jaw gripper is re-sized for grasping work (See Fig 6) from [3]. Two pieces of foams are attached

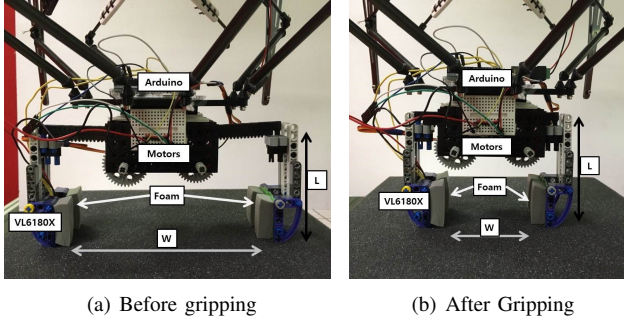


Fig. 6. LEGO-Based parallel gripper concept design

on each side to improve grasping characteristics. The gripper is operated by servomotors that react to tactile feedback from an inter-integrated-circuit (I^2C) compatible sensor, VL6180X (STMicroelectronics). The sensor is mounted left bottom side of the gripper in-hand. An I^2C compatible Arduino-Uno is used to operate the gripper and receive proximity range data from the sensor. The grasping begins when the sensor receives proximity range data from the object. The gripper is mounted end-effector of the parallel manipulator.

E. Parallel-Mechanism Manipulator and Gripper Re-size Criteria

Several factors were considered while re-sizing the parallel-mechanism manipulator and gripper (PMG). The Q450 quadrotor was selected to fly the manipulator because of its better mobility than the previous concept. (See Fig 7) The payload of Q450 is estimated to be $4.5kg$ [13]. Therefore the target weight of the PMG is $1kg$ considering the weights of other components (battery, frame, and etc) or less. In addition, it is important to minimize torque on the UAV from the manipulator. Also, all motors to be mounted rigidly on the manipulator. Therefore the impact on the UAV's stability is minimized by the manipulator. The final design of PMG consists of a manipulator and a gripper with a total mass of $0.705kg$ and a moving mass of $0.337kg$.

The shape of quadrotor also affected manipulator design. The overall shape was changed from rectangular to square. The position of each leg on the base platform, ψ_{bi} and γ_i , were selected to ensure that the manipulator arms do not contact the quadrotor's landing gears while stowed and deployed.

Furthermore, it would be desirable to allow the manipulator lay against the base. This would facilitate grasping work within the limited workspace under the quadrotor ($25cm$ high). To enable this, the relationship between D_1 and D_2 was calculated in Eq. 4

$$D_1 = ||k_i^* - b_i||, \quad (4)$$

where:

$$k_i^* = \begin{bmatrix} k_{xi}^* \\ k_{yi}^* \\ k_{zi}^* \end{bmatrix} = \begin{bmatrix} D_1 \cos(\psi_{bi} \pm \gamma_i) \cos(\theta_i) + b_{xi} \\ D_1 \sin(\psi_{bi} \pm \gamma_i) \cos(\theta_i) + b_{yi} \\ D_1 \sin(\theta_i) + b_{zi} \end{bmatrix} \quad (5)$$

with $\theta_i = 0$.

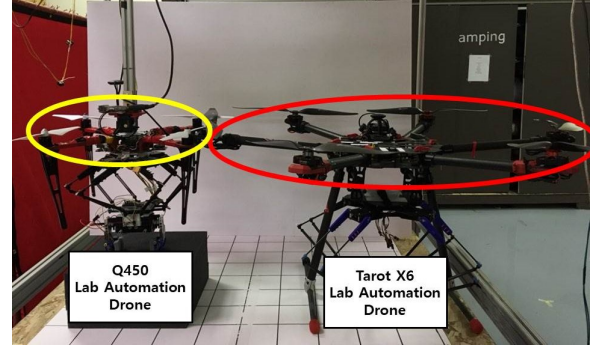


Fig. 7. The current(left) and the previous(right) concept

Lastly, the gripper height is changed to be $11cm$. Grasping range is not changed. The physical properties of the gripper are listed in Table V. The gripper then is attached on the manipulator's end-effector.

IV. EXPERIMENTAL RESULTS

For testing, the PMG attached quadrotor is affixed to a gantry system. A $90cm \times 60cm$ rectangular coordinate system was positioned below the PMG to measure the accuracy of translation. The micro-plate is placed on the top of black-cube. The PMG descends $10cm$ and grasps micro-plates, then delivered to the target location. During the test, an empty micro-plate, a micro-plate with vitamin pills, and a micro-plate with juice sample are delivered from $(80,20,15)$ to $(20,20,15)$.

Table VI describes the revolute joint angles on each leg during the experiments, calculated from Eq. 3. The 8 revolute joint angles are results in same number because the shape was changed to square from previous rectangular design.

TABLE VI
ROTATION ANGLE OF REVOLUTE JOINT

| Positions | | | |
|--------------------|----------------------|--------------|----------------------|
| Store and Delivery | | Pick-up | |
| Joint(i) | θ_i (radians) | Joint(i) | θ_i (radians) |
| 1-8 | 0.0015 | 1-8 | 0.6881 |

Figure. 8- 10 shows the results. Step 6 of each tests show that the design delivered micro-plates gently. There was no damage to test materials. The micro-plate is placed on target positions precisely, which is already tested on the previous work (around 95 percents precision) [3].

V. CONCLUSION AND FUTURE WORK

In this paper, a 6 DOF parallel manipulator with a sensorized parallel jaw gripper from [3] was re-sized for lab automation drone in high throughput systems. A 4 degree of freedom gantry crane was built to emulate rotorcraft motions in a HTS workspace. The experimental results show the re-sized design facilitates micro-plate positioning and orienting with different types of samples.

Future work will consist of more testing and evaluation. The mechanism and design of the manipulator and sensorized

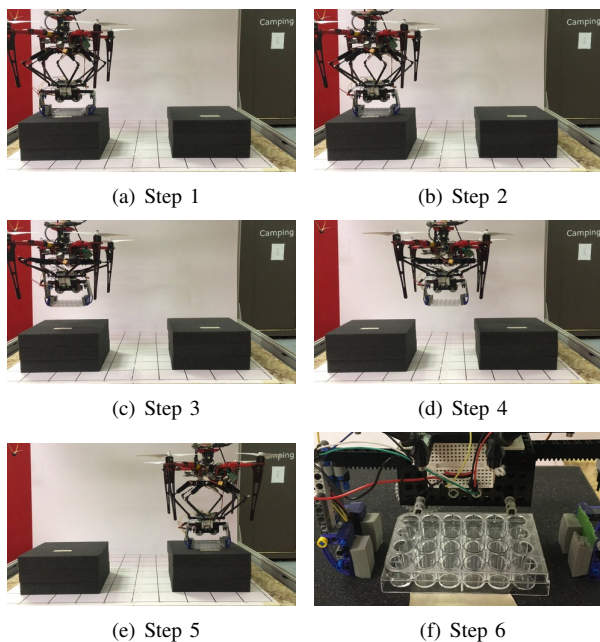


Fig. 8. Empty Micro-plate delivery

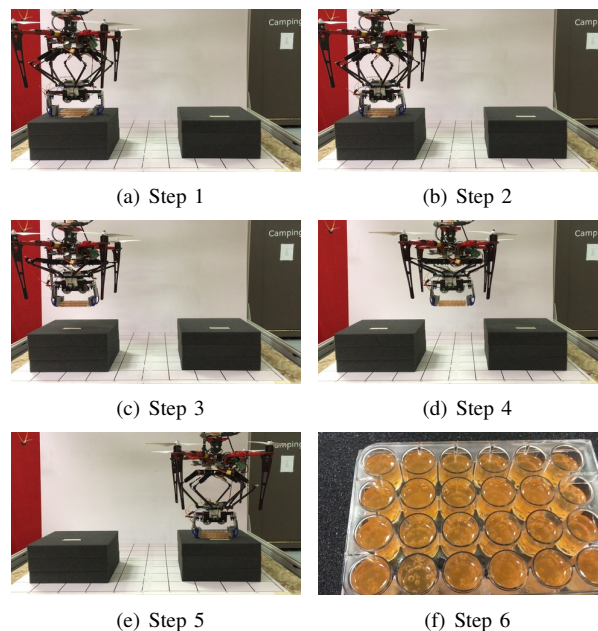


Fig. 10. Micro-plate with juice sample delivery

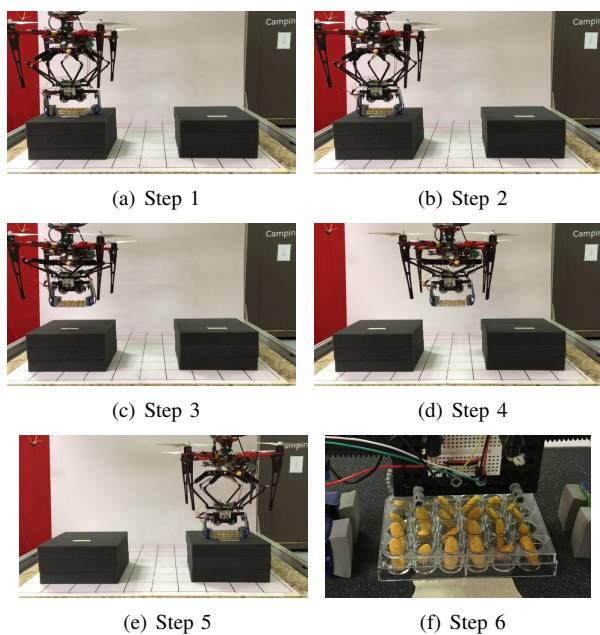


Fig. 9. Micro-plate with vitamin pills delivery

jaw gripper will be addressed. Then, the final design will be affixed on a UAV and deployed inside a mock HTS environment for more variable sample delivery tasks.

REFERENCES

- [1] Sneider, Walter (1985) Drug Discovery: The Evolution of Modern Medicines. John Wiley and Sons, New York, NY
- [2] William P. Janzen (2002) High Throughput Screening : Methods and Protocols. Humana Press
- [3] D. Kim, P. Y. Oh, "Lab Automation Drones for Mobile Manipulation in High Throughput Systems", in Consumer Electronics(ICCE), 2018 International Conference on., IEEE, 2018

- [4] S. Michael, D. Auld, C. Klumpp, et al., "Technology Review - A Robotic Platform for Quantative High-Throughput Screening.", ASSAY and Drug Development Technologies, Volume 6, Number 5, 2008, DOI: 10.1089/adt.2008.150
Available : <http://lifesciences.tecan.com/products/>
- [5] RX160 6-axis industrial robot, STAUBLI[Online]
Available : <https://www.staubli.com/en/robotics/6-axis-scara-industrial-robot/medium-payload-6-axis-robot/6-axis-industrial-robot-rx160/>
- [6] Q. Lindsey, D.Mellinger, and V. Kumar, "Construction of cubic structures with quadrotor teams," Proc. Robotics: Science and Systems VII, 2011
- [7] M. Orsag, C. Korpela, S. Bogdan, and P. Oh, "Valve turning using a dual-arm aerial manipulator," in Unmanned Aircraft Systems(ICUAS), 2014 International Conference on. IEEE, 2014, Pp. 836-841
- [8] T. W. Danko and P.Y. Oh, "Design and control of a hyper-redundant manipulator for mobile manipulating unmanned aerial vehicles," Journal of Intelligent and Robotics Systems, Pp. 1-15, 2013
- [9] D. Mellinger, Q. Lindsey, M. Shomin, and V. Kumar, "Design, modeling, estimation and control for aerial grasping and manipulation," in Intelligent Robots and Systems(IROS), 2011 IEEE/RSJ International Conference on. IEEE, 2011, pp. 2668-2673
- [10] C. Korpela, T. W. Danko, and P. Y. Oh, "Designing a System for Mobile Manipulation from an Unmanned Aerial Vehicle," Technologies for Practical Robot Applications (TePRA), 2011 IEEE Conference on. IEEE, 2011, pp. 109-114
- [11] T. W. Danko, K. P. Chaney, and P. Y. Oh, "A Parellel Manipulator for Mobile Manipulating UAVs," Technologies for Practical Robot Applications (TePRA), 2015 IEEE International Conference on. IEEE 2015, pp.1-6
- [12] F. Szufnarowski, "Stewart platform with fixed rotary actuators a low cost design study," Advances in Medical Robotics, 2013
- [13] J. Sedden, Ph.D. (1990), Basic Helicopter Aerodynamics